A transition state real wave packet approach for obtaining the cumulative reaction probability

Kelsey M. Forsythe and Stephen K. Gray
Chemistry Division, Argonne National Laboratory, Argonne, Illinois 60439

(Received 24 September 1999; accepted 8 November 1999)

We show how the transition state wave packet method of Zhang and Light can be applied within a real wave packet formalism. We also implement random superpositions into the approach, as in the recent work of Matzkies and Manthe, which can significantly reduce the number of propagations at higher temperatures. The net result is a very efficient approach for calculating the cumulative reaction probability, and hence the thermal rate constant, for bimolecular chemical reactions. Full dimensional quantum calculations, including all relevant total angular momenta, of the cumulative reaction probability and thermal rate constant for the $D+H_2 \rightarrow HD+H$ are used as illustration. [S0021-9606(00)01205-8]

I. INTRODUCTION

The cumulative reaction probability, especially through the work of Miller and co-workers,[1–6] has been established to be a very useful tool in chemical reaction rate theory. Numerous other researchers have also utilized cumulative reaction probability ideas to obtain accurate[7–13] and approximate[14–17] theoretical approaches to chemical reaction rates. For a bimolecular chemical reaction, the cumulative reaction probability as a function of total energy, $N(E)$, is defined to be the sum of all possible reactive quantum transition probabilities $P_{n_r,n_p}(E)$,

$$N(E)=\sum_{n_r,n_p} P_{n_r,n_p}(E), \tag{1}$$

where n_r and n_p denote sets of reactant and product quantum numbers. The bimolecular thermal rate constant $k(T)$ is a Boltzmann average of $N(E)$,

$$k(T)=\frac{1}{2\pi\hbar Q_r(T)}\int dE e^{-E/k_BT}N(E), \tag{2}$$

where Q_r denotes the partition function of the reactants. The main idea is to find more efficient or direct approaches to computing $N(E)$ than the explicit sum over all the allowed state-to-state transitions indicated in Eq. (1). In particular, much progress has been made using the following, alternative definition for $N(E)$ due to Miller, Schwartz, and Tromp[2]:

$$N(E)=\frac{(2\pi\hbar)^2}{2}\mathrm{tr}[\,\delta(E-H)F\,\delta(E-H)F], \tag{3}$$

where H is the Hamiltonian operator and F is a flux operator consistent with a surface separating reactant and product regions.

The transition state wave packet (TSWP) method, introduced by Zhang and Light,[7–10] is a physically appealing, time-dependent approach to calculating $N(E)$. It involves propagating a set of wave packets localized in a transition state region. The corresponding expression for $N(E)$ involves a sum over transition state wave packet contributions and, depending on the nature of the potential surface, fewer transition state wave packets than number of terms on the right-hand side of Eq. (1) might be needed. However, even if this is not the case, the use of discrete variable representations (DVRs),[18–21] and absorbing boundary conditions (ABC),[22,23] can still yield considerable computational savings in relation to initial state selected wave packet (ISSWP) propagation approaches. Of course, such ''DVR-ABC'' ideas, coupled with sparse matrix linear algebra methods, allow one to compute $N(E)$ efficiently with time-independent methods as well.[3–6] There tends to be a blurring of the distinction between time-dependent and time-independent methodologies when common strategies and numerical techniques are employed.[24] This will also be illustrated in the present work.

The TSWP method, in its most straightforward form, involves propagation of complex valued wave packets. Most time-independent approaches to $N(E)$ make use of complex Green's functions or optical potentials and therefore also involve complex vectors. We show here, however, that it is possible to propagate just the real part of complex wave packets, and from just the real part infer all the relevant information for construction of $N(E)$. This can halve the amount of computer time and memory required to obtain $N(E)$ in relation to the straightforward approach. This represents an application of the ''real wave packet'' formalism outlined by Gray and Balint-Kurti,[24] which also makes use of the fact, pointed out by Meijer *et al.*,[25] that reactive fluxes can be inferred from real wave packet propagation. Additional savings, particularly for high temperatures where many transition state wave packets are required to converge rate constants, is provided by adopting statistical initial condition sampling methods as in the work of Matzkies and Manthe.[13]

Section II outlines our approach to $N(E)$, Sec. III presents and discusses a full dimensional determination of $N(E)$ and $k(T)$ for the $D+H_2 \rightarrow HD+H$ reaction, and Sec. IV concludes.

II. TRANSITION STATE REAL WAVE PACKET (TS-RWP) APPROACH

Section II A outlines the necessary aspects of the real wave packet formalism.[24,25] Section II B shows how one can then apply Zhang and Light's TSWP approach.[7–10] Section II C discusses aspects of TSWP initial state selection, including the idea of random superpositions.[13]

A. Real wave packet formalism

Two observations in Ref. 24 were (i) it is possible to infer reaction probabilities from just the real part of an evolving wave packet, and (ii) the wave packet can be generated from a modified time-dependent Schrödinger equation with the Hamiltonian operator H replaced by $f(H)$, where the functional form of $f(H)$ is chosen for convenience. [$f(H)$ should, of course, be a Hermitian operator and in order for one to focus on just the real part of a wave packet one must have a real symmetric matrix representation for $f(H)$.]

Let $\phi(t)\equiv\phi(\mathbf{x},t)$ be a (complex) wave packet satisfying

$$i\hbar\frac{\partial}{\partial t}\phi(t)=f(H)\phi(t). \tag{4}$$

Let $f_E\equiv f(E)$ denote the eigenvalues of $f(H)$. Energy (or equivalently f_E) resolved observables may be estimated with the aid of integrals of the form

$$I(f_E)=\int_{-\infty}^{+\infty}dt e^{if_E t/\hbar}\phi(t). \tag{5}$$

For example, the coordinate ($\mathbf{x}$) dependence of such integrals can be used with flux approaches to calculate energy resolved reaction probabilities.[25] If one can assume $I(f_E)$ is one-sided in f_E, i.e., there is no amplitude for either $f_E>0$ or $f_E<0$, then it is easy to show $I(f_E)$ may also be obtained from just the real part of $\phi(t)$, $q(t)=\mathrm{Re}\,\phi(t)$, according to[24,25]

$$I(f_E)=2\int_{-\infty}^{+\infty}dt e^{if_E t/\hbar}q(t). \tag{6}$$

The one-sided condition is not difficult to satisfy. For example, with the Chebyshev iteration[26] variation of the real wave packet idea (see below) it is automatically satisfied.[24]

If one chooses $f(H)=H$, i.e., considers the usual Schrödinger equation, an efficient scheme for obtaining just the real part of the wave packet has been previously outlined,[27] and this could be used if desired. Conceptually, this is the simplest approach. However, we believe a more efficient approach is to assume

$$f(H)=-\frac{\hbar}{\tau}\arccos(H_s), \tag{7}$$

where $H_s=a_s H+b_s$ is a scaled Hamiltonian operator (or matrix in applications) which has eigenvalues within $[-1,1]$, coupled with a relatively stable form of absorption.[24,27] This results in q satisfying a simple recursion,

$$q^{(k+1)}=A[-Aq^{(k-1)}+2H_s q^{(k)}], \tag{8}$$

with $k=1,2,\ldots$ denoting the discrete time steps $t=k\tau$ and where A denotes a suitable rule for absorption in reactant and product coordinate regions. The time step τ turns out to be arbitrary and cancels out of any expression for a reaction probability. Equation (8) is the same damped Chebyshev iteration as introduced in the time-independent work of Mandelshtam and Taylor.[28] See also the time-independent wave packet ideas of Kouri and co-workers.[29] The real wave packet approach, as it applies to Eq. (7), can therefore be also viewed as a variation on these time-independent approaches that applies standard wave packet initial conditions and analysis methods to the Chebyshev iterates.

Note if the initial condition $\phi(t=0)$ is complex, there is no difficulty in applying the formalism.[24,30] Equation (8) requires knowledge of $q^{(0)}$ and $q^{(1)}$ to be initiated. If $q^{(0)}=\mathrm{Re}\,\phi(t=0)$ and $p^{(0)}=\mathrm{Im}\,\phi(t=0)$, $q^{(1)}$ is obtained from $q^{(1)}=H_s q^{(0)}-\sqrt{1-H_s^2}\,p^{(0)}$, where the act of the square root operator on $p^{(0)}$ can be evaluated with, e.g., a Chebyshev expansion. (Typically the required number of terms in the expansion is much less than the number of iterations required to compute observables.)

A new aspect of the present work is the necessity to propagate backward in time. This is accomplished through the following backward Chebyshev iteration,

$$q^{(k-1)}=A[-Aq^{(k+1)}+2H_s q^{(k)}], \tag{9}$$

where now $k=-1,-2,\ldots$ In this case one needs $q^{(0)}$ and $q^{(-1)}$ to initiate the iteration with $q^{(-1)}=H_s q^{(0)}+\sqrt{1-H_s^2}\,p^{(0)}$.

B. Transition state wave packets

Zhang and Light,[7] starting from Eq. (3), arrived at an expression for $N(E)$ involving a sum over transition state wave packet (TSWP) contributions,

$$N(E)=\sum_i N_i(E), \tag{10}$$

with

$$N_i(E)=\langle\psi_i(E)|F_{s_0}|\psi_i(E)\rangle, \tag{11}$$

where the flux operator F_{s_0} can be written in terms of some appropriate coordinate s and its associated momentum operator p_s as

$$F_{s_0}=\frac{1}{2\mu_s}[\delta(s-s_0)p_s+p_s\delta(s-s_0)]. \tag{12}$$

The condition $s=s_0$ is assumed to define a surface separating reactant and product regions of space. The energy resolved TSWPs are given by

$$\begin{aligned}\psi_i(E)&=2\pi\hbar\sqrt{\lambda}\,\delta(E-H)\phi_i(t=0)\\&=\sqrt{\lambda}\int_{-\infty}^{+\infty}dt e^{iEt/\hbar}\phi_i(t),\end{aligned} \tag{13}$$

where $\phi_i(t)=\exp(-iHt/\hbar)\phi_i(t=0)$ and λ is the positive eigenvalue of the flux operator (see Sec. II C). Notice that both forward and backward propagations of the initial condition $\phi_i(t=0)$ are required to evaluate Eq. (13).

The simplest way to obtain the corresponding real wave packet interpretation involves setting

$$\delta(E-H)=\left|\frac{df_E}{dE}\right|\delta[f_E-f(H)], \tag{14}$$

which allows us to replace Eq. (13) with

$$\psi_i(E)=2\pi\hbar\left|\frac{df_E}{dE}\right|\sqrt{\lambda}\,\delta[f_E-f(H)]\phi_i(t=0)$$

$$=\left|\frac{df_E}{dE}\right|\sqrt{\lambda}\int_{-\infty}^{+\infty}dt e^{if_E t/\hbar}\phi_i(t), \tag{15}$$

where now $\phi_i(t)=\exp(-if(H)t/\hbar)\,\phi_i(t=0)$ is a solution of Eq. (4).

Using Eq. (15), each TSWP contribution, Eq. (11), can be written as

$$N_i(E)=\frac{\lambda\hbar}{\mu_s}\left|\frac{df_E}{dE}\right|^2\mathrm{Im}\left\langle\int_{-\infty}^{+\infty}e^{if_E t/\hbar}\phi_i(t)dt\right|$$

$$\times\int_{-\infty}^{+\infty}e^{if_E t'/\hbar}\frac{\partial}{\partial s}\phi_i(t')dt'\Big\rangle_{s=s_0}, \tag{16}$$

where we have also used the definition of the flux operator, Eq. (12). All quantities within the inner product are fixed on the surface defined by $s=s_0$ and the inner product is an integration over the remaining spatial variables.

The subsequent analysis then parallels the development in Ref. 25. If just the real part of each TSWP, $q_i(t)=\mathrm{Re}\,\phi_i(t)$, is available, then Eq. (6) implies that Eq. (16) becomes

$$N_i(E)=\frac{4\lambda\hbar}{\mu_s}\left|\frac{df_E}{dE}\right|^2\mathrm{Im}\left\langle\int_{-\infty}^{+\infty}e^{if_E t/\hbar}q_i(t)dt\right|$$

$$\times\int_{-\infty}^{+\infty}e^{if_E t'/\hbar}\frac{\partial}{\partial s}q_i(t')dt'\Big\rangle_{s=s_0}. \tag{17}$$

Assuming $f(H)$ is given by Eq. (7), which implies the $q_i(t)$ are generated by the Chebyshev iterations Eq. (8), leads to

$$N_i(E)=\frac{4\lambda a_s^2\hbar^3}{\mu_s(1-E_s^2)}\mathrm{Im}\left\langle\sum_{k=-\infty}^{\infty}e^{i\theta_E k}q_i^{(k)}\right|$$

$$\times\sum_{k'=-\infty}^{\infty}e^{i\theta_E k'}\frac{\partial}{\partial s}q_i^{(k')}\Big\rangle_{s=s_0}, \tag{18}$$

where $\theta_E=-\arccos(E_s)$, $E_s=a_sE+b_s$. Equation (18) is the main equation used in our calculation of $N(E)$. It is possible to obtain similar (but not exactly the same) expressions via Chebyshev expansion of the $\delta(E-H)$ terms in $N(E)$. This is perhaps more in the spirit of the time-independent wave packet ideas[28,29] and we outline this approach, as well as a connection with real wave packet propagation, in the Appendix.

C. Initial conditions and sampling

The TSWP method differs from standard initial state selected wave packet (ISSWP) propagation schemes in the choice of initial conditions. Instead of sampling from a distribution of asymptotic reactant states, one chooses instead from a set of states localized in a transition state region.[7] Formally, we can think of a condition $s=s_{TS}$ on some suitable reaction coordinate as defining the effective transition state region. It is important to note that the surface defined by $s=s_{TS}$ need not be the same as the surface ($s=s_0$) used for carrying out the flux analysis to obtain the various $N_i(E)$.[7]

The initial TSWPs, $\phi_i(t=0)$, are defined as

$$\phi_i(\mathbf{x},t=0)=\chi(s)\,\eta_i(\mathbf{u}), \tag{19}$$

where we divide the coordinates $\mathbf{x}$ into the assumed transition state coordinate s and the remaining degrees of freedom $\mathbf{u}$. $\chi(s)$ is the eigenfunction of a flux operator, $F_{s_{TS}}|\chi\rangle=\lambda|\chi\rangle$, for which $\lambda>0$. Within a finite basis or grid representation, $\chi(s)$ will be strongly peaked at $s=s_{TS}$. [Note that the simple one-dimensional flux operator we use, Eq. (12), when diagonalized in an L^2 basis, leads to just two nonzero eigenvalues λ and $-\lambda$, with all other eigenvalues being zero. Other forms for the flux operator may have more nonzero eigenvalues than this.[31,32]] The set of internal functions $\{\eta_i(\mathbf{u})\}$ must provide a complete description of the coordinates orthogonal to s, and can be vibration-rotation eigenfunctions of some appropriate reduced Hamiltonian model (see, e.g., Sec. III B). Of course, one can vary the choice of s_{TS} with the hope of finding a value such that the total number of available internal states less than some maximum energy is a minimum. For reactions with tight transition states or high barriers, this number of states could be less than the total number of ISSWPs one would have to propagate to evaluate Eq. (1).[7]

The simplest approach to the evaluation of Eq. (18) is to systematically progress through the initial TSWPs given above, with $i=1,\ldots,M$, with i increasing such that the η_i correspond to ever higher energy internal states and to stop at some M when convergence is achieved. An alternative is to use statistical sampling as in the work of Matzkies and Manthe.[13] (See also related work by Jeffrey and Smith.[33]) In the present context the idea is as follows. Equation (10) is replaced by the average over N_{rs} or number of random superpositions

$$\tilde{N}_{\mathrm{avg}}(E)=\frac{1}{N_{rs}}\sum_{k=1}^{N_{rs}}\tilde{N}_k(E), \tag{20}$$

where

$$\widetilde{N_k}(E)=\langle\widetilde{\psi_k}(E)|F_{s_0}|\widetilde{\psi_k}(E)\rangle, \tag{21}$$

with each $\widetilde{\psi_k}(E)$ being an energy resolved state determined via Fourier transformation of a time-dependent state $\tilde{\phi}_k(t)$ in a manner analogous to Eq. (13) or Eq. (15). However, the corresponding initial condition $\tilde{\phi}_k(t=0)$ is given by a random superposition of M TSWPs,

$$\widetilde{\phi_k}(t=0)=\sum_{i=1}^{M}(-1)^{\alpha_i^k}\phi_i(t=0), \tag{22}$$

with the α_i^k being a random sequence of 0's and 1's.

Equation (21) becomes

$$\widetilde{N}_k = \sum_{i,j} (-1)^{\alpha_i^k}(-1)^{\alpha_j^k}\langle\psi_i|F_{s_0}|\psi_j\rangle. \tag{23}$$

The relation[13]

$$\delta_{ij} = \lim_{N_{rs}\to\infty} \frac{1}{N_{rs}} \sum_{k=1}^{N_{rs}} (-1)^{\alpha_i^k}(-1)^{\alpha_j^k}, \tag{24}$$

transforms $\widetilde{N_{rs}}$ in the limit of a large number of random superpositions, into $N(E)$,

$$\lim_{N_{rs}\to\infty} \widetilde{N}_{\text{avg}}(E) = \sum_{i=1}^{M} \langle\psi_i|F_{s_0}|\psi_i\rangle = N(E). \tag{25}$$

M, the total number of transition state wave packets employed in the random superpositions, depends on the energetic range of interest. Ideally, in certain situations $N(E)$ can be estimated to some desired accuracy by propagating $N_{rs} < M$ random superpositions.

III. APPLICATION TO D+H$_2$

To illustrate the methodology of Sec. II, we obtain the cumulative reaction probability and bimolecular rate constant for the D+H$_2$→HD+H reaction, in three dimensions, including all relevant angular momenta. The Liu-Siegban-Truhlar-Horowitz (LSTH) potential energy surface[34–36] is employed. This application was chosen so that we can then compare to the accurate and extensive results of Mielke *et al.*[37]

A. Representation

In our calculations, we represent the wave packet and Hamiltonian in terms of reactant Jacobi coordinates: R, the distance from D to the H$_2$ center of mass; r, the H$_2$ internuclear distance; and cos γ, the cosine of the angle between vectors associated with R and r. A body-fixed (BF)[38–40] representation is employed which introduces Ω, the projection of total angular momentum on the R axis. Without external forces there are three conserved quantum numbers: the total angular momentum quantum number J, the projection quantum number for total angular momentum on a space-fixed (SF) z-axis M, and the parity quantum number p (0 or 1). Because the results are independent of M we suppress explicit reference to this quantum number in what follows. Within the BF representation, a wave packet or its real part q may then be expanded as[39,40]

$$q^{J,p}(R,r,\cos\gamma,t;\boldsymbol{\alpha}) = \sum_{\Omega=\Omega_{\min}}^{J} \sum_{j\geqslant\Omega}^{j_{\max}} C_{j,\Omega}^{J,p}(R,r,t) G_{j,\Omega}^{J,p}(\cos\gamma;\alpha), \tag{26}$$

where the $G_{j,\Omega}^{J,p}$ are parity adapted angular functions that involve associated Legendre polynomials in cos γ and Wigner matrices in three Euler angles (denoted collectively as α), as in Refs. 39 and 40. $\Omega_{\min}$ in Eq. (26) can be either 0, in which case there are $J+1$ coupled Ω states, or 1, in which case there are J coupled Ω states. The two possible choices for $\Omega_{\min}$ determine the two different parity cases, with it being the case that if there is an odd number of Ω states the parity $p=0$ (even) and if there are an even number of Ω states the parity $p=1$ (odd).[39]

TABLE I. Grid and related parameters for the three-dimensional D+H$_2$ calculations.

Parameter	J=0–4	J=5–25
H$_2$ distance, r/a_0	0.5–5.5	0.5–7.5
Number of grid points in r	25	37
Distance between D and the center of H$_2$, R/a_0	0–5	0–7
Number of grid points in R	27	37
Number of (even) diatomic rotational states, j	16	16
Potential and centrifugal cutoffs, V_{cut}/eV	6	6
Coriolis cutoff/eV	3	3
Absorption in R starts at R_a/a_0	3.0	4.0
Absorption in r starts at r_a/a_0	3.0	4.0
Absorption strength in R, c_R/a_0^{-2}	0.01	0.01
Absorption strength in r, c_r/a_0^{-2}	0.01	0.01
Flux analysis point, r_0/a_0	3.0	4.0

The Hamiltonian operator H may be written formally as

$$H = \frac{P_R^2}{2\mu_R} + \frac{p_r^2}{2\mu_r} + \frac{(\mathbf{J}-\mathbf{j})^2}{2\mu_R R^2} + \frac{\mathbf{j}^2}{2\mu_r r^2} + V(R,r,\cos\gamma), \tag{27}$$

where $\mu_R = m_D 2m_H/(m_D+2m_H)$, $\mu_r = m_H/2$, P_R and p_r are appropriate radial momentum operators associated with R and r, and $\mathbf{J}$ and $\mathbf{j}$ denote the (vector) total angular momentum and H$_2$ angular momentum operators.

The forward and backward propagations with Eqs. (8) and (9), for practical purposes, amount to updating the channel coefficients $C_{j,\Omega}^{J,p}(R,r,t)$. This involves, per step, one act of H on a real vector $q^{J,p}$. As in previous work,[39,40] $Hq^{J,p}$ breaks down into three parts. First, one has the diagonal (in j and Ω) contributions from the kinetic energy: the actions of the radial kinetic operators $P_R^2/2\mu_R$ and $p_r^2/2\mu_r$ on the channel coefficients, as well as multiplication by the centrifugal terms that result from the angular kinetic energy operators. Second, one has Coriolis coupling terms, resulting from the $(\mathbf{J}-\mathbf{j})^2$ term in Eq. (27), which couple Ω to $\Omega\pm1$. Third, one has the action of the potential, which is diagonal in Ω, but off-diagonal in j. The relevant equations may be found in numerous references, including Refs. 39 and 40. We use evenly spaced grids in R, and r, coupled with fast Fourier sine transformations to evaluate the radial kinetic energy terms. Rather than store large matrices of the potential in terms of the relevant associated Legendre basis functions, we simply carry out, for each Ω, j, R, and r, a transformation from the associated Legendre basis to a Gauss-Legendre quadrature[41] in terms of cos γ grid points, multiply the result by the actual potential values on the grid points, and transform back to the associated Legendre basis.[24]

Table I lists the grid and basis set details associated with our propagations. The grid details change with increasing J owing to the increased importance of long range effects. We found that larger grids were necessary at the intermediate to higher J values to minimize artificial reflection effects. The absorption parameters in Table I correspond to damping the channel packets according to $A(R,r)=A_R(R)A_r(r)$ (for all

Ω and j), with $A_x = \exp[-c_x(x-x_a)^2]$ whenever $x > x_a$ with $x = R$ or r. Energetic cutoffs were also introduced, which reduce the spectral range of the Hamiltonian and therefore reduce the number of iterations required.[24] Note that we apply an energetic cutoff not only to the potential energy, but also to the centrifugal terms and the magnitude of Coriolis coupling terms. The latter terms tend to $-\infty$ as R tends to 0. (Care must be taken to ensure the magnitude of the cutoff is sufficient so that no imbalance between the centrifugal and Coriolis terms results.)

For each $J > 0$ considered, we carry out calculations for both parity cases, corresponding to whether or not $\Omega = 0$ is included in the basis, as discussed below Eq. (26). In fact, it is important to note that there can be relatively large differences in the reactivity associated with different parities, even for J as high as $J = 20$, with it generally being the case that the parity such that $\Omega = 0$ is included in the basis yields a higher cumulative reaction probability. In addition to parity, the hydrogen atom exchange symmetry allows one to decouple $j = 0, 2, 4, \ldots$ and $j = 1, 3, 5, \ldots$ cases, which also correspond to the nuclear para and ortho states, respectively. (Note that it is straightforward to reduce similarly the number of angular grid points used in the evaluation of the action of the potential if j is restricted to be even or odd.[42]) While the results are sensitive to the overall parity, it has been previously demonstrated[37] that cumulative reaction probabilities (and rate constants) for $D + H_2$ associated with only ortho and only para states are equivalent to within a few percent, so we restrict attention to the even j (para) case.

B. Determination of the initial TSWPs and propagation

For simplicity, we take the reaction coordinate s of Sec. II C to be simply the H_2 internuclear distance, r, for which a moderately large value can be taken to be the condition for dividing reactants and products. The remaining variables R, $\cos\gamma$, and the Euler angles α or, effectively, the set of allowed Ω values for each J, constitute the remaining variables $\mathbf{u}$. Of course other choices for s and $\mathbf{u}$, based, e.g., on certain rotations of the original reactant Jacobi coordinates, might be better[7] both in terms of minimizing the total number of TSWPs and in terms of minimizing the size of the grid representation.

With $s = r$, $F_{r_{TS}}$ is easily diagonalized numerically in a basis of a one-dimensional particle in a box wave functions, and the relevant eigenvector $\chi(s = r)$ associated with the positive eigenvalue $\lambda > 0$ of $F_{r_{TS}}$ is obtained. This eigenvector is highly localized on $r = r_{TS}$ and contains a broad range of energies. (Note that the flux operator has some curious properties, including the fact that λ increases in magnitude as the basis set increases).[43,44]

With $\mathbf{u} = (R, \cos\gamma, \{\Omega\})$, the internal states $\eta_i(\mathbf{u})$ of Sec. II C are then simply the eigenstates of the appropriate, reduced dimensional Hamiltonian operator obtained by holding $r = r_{TS}$ in Eq. (27) and omitting the associated $p_r^2/2\mu_r$ kinetic energy term. If E represents the largest total energy of interest, determined by the largest temperature T of interest, the optimum value of the reaction coordinate (r_{TS}) is the one that leads to the lowest number of TSWPs with internal energies (i.e., eigenvalues of the reduced dimensional Hamiltonian) less than some maximum E. Typically, we find $r_{TS} \approx 2.4\ a_0$, which is slightly larger than the actual collinear transition state value of $1.76\ a_0$. For $J = 0, 1, \ldots, 10$ and R grid sizes of 27–37, corresponding to reduced dimension Hamiltonian matrices ranging in size from 432 to 5402, we used a direct diagonalization procedure (the Jacobi method).[45] However, for larger J it becomes computationally prohibitive to diagonalize the matrices directly and so we used an iterative matrix eigenvalue method to obtain just the eigenvalues and eigenvectors of relevance. The particular iterative method used was the implicitly restarted Lanczos (or more generally Arnoldi) method,[46] for which there is very robust, freely available software.[47]

We propagate the real part, q, of each initial TSWP (or each random superposition of TSWPs) forward and backward according to Eqs. (8) and (9). After each propagation (or iteration) step, the $r = r_0$ portions of q and its derivative with respect to r, $\partial q/\partial r$, are written to files for later analysis with Eq. (18). We employ an analysis surface condition $r = r_0 = 3 - 4a_0$, which is different from, and toward the product side of the condition we use to define the TSWPs, $r = r_{TS} \approx 2.4a_0$. Note that the individual $N_i(E)$ do depend on the analysis surface position, with only their sum, $N(E)$, *if* it is converged, being invariant to any surface that separates reactants from products.

For our main calculations, with the grid, absorption, and other parameters listed in Table I, 400 forward and 400 backward iteration steps suffice to converge $N(E)$, or its total angular momentum resolved variants, to within a few percent. However, a difficulty arises in the deep tunneling limit where $N(E)$ becomes exponentially small with decreasing energy E. This difficulty, which becomes apparent for $N(E)$ with magnitudes $\leqslant 10^{-2}$, cannot even be seen on the scale of the $N(E)$ figures we subsequently present. However, this deep tunneling limit is important in the estimation of $D + H_2$ rate constants with $T \leqslant 300$ K. In principle, much longer time (or iteration) and distance scales than those used in our main calculations become necessary and, furthermore, one must carefully experiment with absorption. Due to imperfections in the absorption, and with our current grid parameters, for example, negative $N(E)$ values can even result. In our calculations we simply omit any negative $N(E)$ values from our rate constant estimations. Of course, two more acceptable alternatives are: (i) to separately treat the low E or T aspect of the problem with more extensive calculations, or (ii) to fit each calculated $N(E)$ just above the deep tunneling limit with an analytical tunneling formula that exhibits more correct behavior for lower E. None of these alternatives is particularly appealing and the difficulty in describing the deep tunneling limit must be considered a negative aspect of both our approach and, we suspect, most DVR-ABC approaches that rely on compact grids coupled with absorption boundaries.

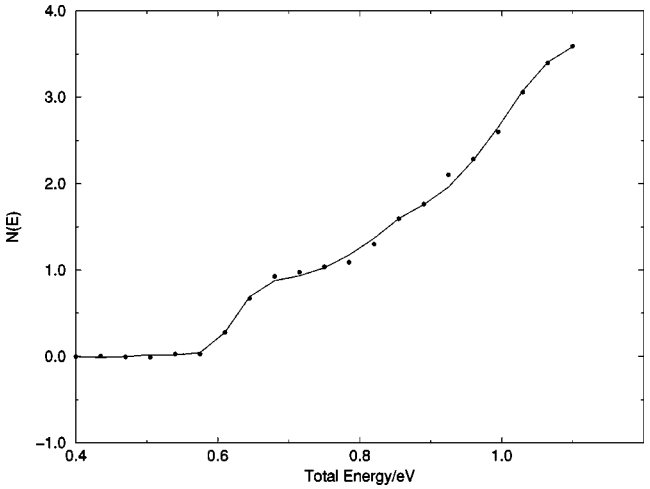

FIG. 1. The J=0 cumulative reaction probability for D+para-H_2 calculated with standard ISSWP approach (solid curve) and TS-RWP (solid circles).

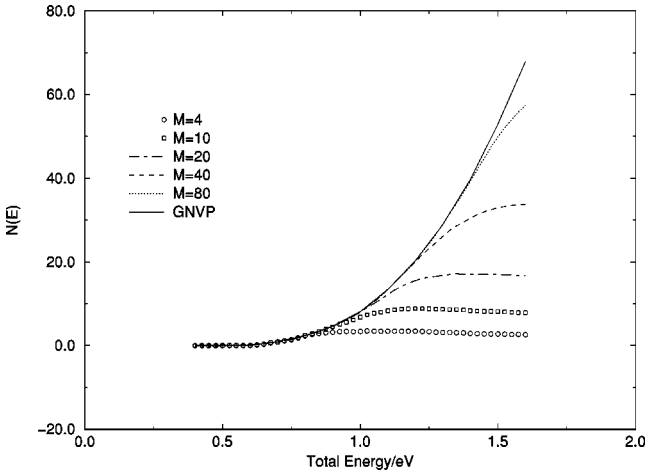

FIG. 2. The J=6 cumulative reaction probability for D+para-H_2 (including both overall parities) calculated via the TS-RWP approach with various numbers, *M*, of TSWPs. The GNVP results of Mielke *et al.* (Ref. 37) are also shown for comparison.

C. Results

The thermal rate constant Eq. (2) can also be written as

$$k(T)=\sum_J (2J+1)k_J(T), \tag{28}$$

where

$$k_J(T)=\frac{1}{Q_r(T)}\int dE N_J(E)e^{-\beta E}, \tag{29}$$

and $N_J(E)$ denotes the cumulative reaction probability determined from a calculation with a specific *J*. We first investigate selected *J* cases. Figure 1 illustrates the cumulative reaction probability for $J=0$. The solid points represent the TS-RWP method of Sec. II and the curve represents a direct determination of the para (i.e., even j) contribution to the cumulative reaction probability [Eq. (1)] using a more standard, initial state selected wave packet (ISSWP) method. The latter calculations were performed with larger grids and the flux based approach of Ref. 25. The TS-RWP results are for six wave packets. The ISSWP calculations required propagating the seven lowest initial rovibrational states of H_2, with the total number of allowed initial states with energy less than 1.1 eV being 10. Thus, in this case the number of TSWPs was not significantly fewer than the number of ISSWPs required to obtain a reasonable $N(E)$. However, the ISSWP calculation involved 127 *R* grid points, 95 *r* grid points, and 16 γ grid points. Comparing to the parameters listed in Table I, this translates into a factor of 16 computational savings with the TS-RWP approach. Naturally, some additional effort could be invested in optimizing the grid and other features of the ISSWP calculations and so this is probably a somewhat optimistic estimate. Nonetheless, individual TSWP propagations with our approach can be quite efficient, particularly for low *J*. For example, a single $J=0$ TSWP requires just 2 CPU minutes to be completely propagated on a 200 MHz IBM RS/6000 workstation. The CPU time also scales linearly with *J*. Figure 2 compares the TS-RWP method to the generalized Newton variational principle (GNVP) calculations of Mielke *et al.*[37] for $J=6$. One can see how the TS-RWP results converge as the number of TSWPs propagated, in order of increasing internal energy, is increased from $M=4$ to 80 (i.e., 2 to 40 propagations for each even and odd parity case). Note that this $J=6$ case involves considerably more TSWPs than the corresponding $J=0$ case. This is because the energy range considered is greater (1.6 compared to 1.1 eV) and the density of states increases dramatically as one increases energy. The agreement in Fig. 2 is quite good and can be improved at higher total energies by including more wave packets. However, for the temperature range considered in the calculations of thermal rate constants reported below, the energy range spanned by the first 40 transition state wave packets is probably sufficient.

We next consider various *J* selected thermal rate constants as defined in Eq. (29). Recall (Sec. III A) that all our calculations were for only the para contribution to the cumulative reaction probability and, owing to the very similar results previously obtained for ortho and para contributions,[37] we approximate $N_J^{\text{ortho}}(E)\approx N_J^{\text{para}}(E)$, so that $N^J(E)=N^J_{\text{para}}+3N^J_{\text{ortho}}\approx 4N^J_{\text{para}}$ in the evaluation of $k^J(T)$. Figure 3 contrasts our TS-RWP (symbols) results with the accurate GNVP results (curves) of Mielke *et al.*[37] for $J=0$, 3 and 6. One sees, in general, reasonably good agreement between the two calculations on the scale of the figure. For $T\geqslant 500$ K, the differences between the two calculations for all three *J* cases range between 0 and 3%. For the lowest temperature considered, however, our $J=0$ result is more significantly in error by 14%. This error is, in fact, on the order of the contribution to the rate constant from the deep tunneling limit, and reflects the convergence difficulties noted in the last paragraph of Sec. III B.

We now investigate the use of N_{rs} random superpositions of the 40 most energetically important TSWPs (see Sec. II C). Our focus will be on the *J* specific rate constants k_J of Eq. (29). Figure 4 displays how the rate constant converges as one considers different numbers of random superpositions, N_{rs}, and contrasts this with the convergence of the rate constant determined by considering the TSWPs ordered energetically, as in our earlier discussion of Fig. 2. Three

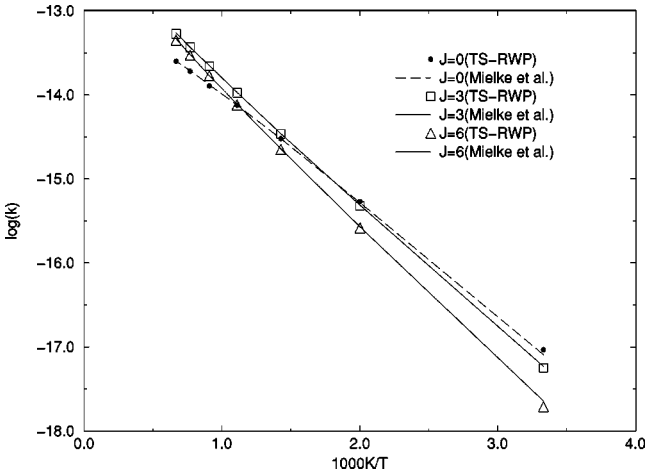

FIG. 3. The logarithm (base 10) of J selected thermal rate constants (units of cm^3 $molecule^{-1}$ s^{-1}) for $D+H_2$ for $J=3$, 6, and 9 calculated via the present approach (TS-RWP) and the GNVP results of Mielke *et al.* (Ref. 37).

different total angular momentum results, $J=9$, 15, and 24 are displayed. While typically $M\approx 40$ (20 for each parity) individual TSWP propagations are necessary to converge each rate constant, after only a few propagations of the random superpositions the result is clearly close, within certain statistical error, to the correct, converged result. This is clear from Fig. 4 in how one sees that propagations of $N_{rs}=4$, 10, and 20 superpositions yield curves that are all quite close to one another. The error bars are given for the case of averaging over only four random superpositions. (Errors were estimated by calculating the rate constant for a given random superposition and calculating the average and variance accordingly.) In contrast, particularly at the higher temperatures, the convergence with respect to propagating TSWPs in energetic order (the isolated points) is less satisfactory. We should note that the scale of Fig. 4 hides the fact that the random superpositions do not converge very quickly at low temperatures when the actual J selected rate constants are of much smaller magnitude. This is illustrated more clearly in Table II, which corresponds to the results for $J=9$ at selected temperatures. One sees that the $T=300$ K result, even at the level of 40 random superpositions, is in error by a factor of 3 in relation to the more converged result based on $M=80$ (40 for each parity) energetically ordered TSWP propagations. Table II also includes comparison with the accurate GNVP results of Mielke *et al.*[37] We see that our $M=80$ (40 per parity) $T=500$ and 700 K results for $J=9$ are in excellent agreement with those of Mielke *et al.*, and the 5% error of our $M=80$ (40 per parity) result at $T=300$ K is consistent with the difficulties previously noted in Sec. III B (and also the discussion of Fig. 3 above), in converging the deep tunneling limit of $N(E)$.

Next we present calculations of the full thermal rate constant. In these calculations, in order to obtain reasonable accuracy at the lower temperatures, we individually propagated $M=20$ (10 per parity) energetically ordered TSWPs for $J=0$–4, and $M=40$ (20 per parity) TSWPs for $J=4$–10. For $J>10$, we employed instead propagations of $N_{rs}=4$–20 (2–10 per parity) random superpositions. (It is very important to include these high J states because they make a 30% to 40% contribution to the total thermal rate constant at the highest temperatures studied here.) Table III compares our calculated thermal rate constants with the accurate GNVP ones of Mielke *et al.*,[37] as well as experimental results.[48] The agreement between the TS-RWP and GNVP results is quite good, with the greatest error, 6%, in the TS-RWP results arising at the lowest temperature $T=300$ K. Note only four (two per parity) random superpositions were employed for $J>10$ for these results. Furthermore, it is important to emphasize that the statistical errors in the total rate constant could have been reduced by including all relevant J states in the random superpositions,[13] and this is probably the optimal way of applying the random superposition idea to estimate a rate constant. We used a different approach — random superpositions for each individual J — so we could also compare with the J specific results of Mielke *et al.*[37]

The results in Table III required ≈400 real wave packet propagations. We did not perform the extensive $J>0$ ISSWP propagations necessary to determine the corresponding number of propagations and actual computational effort required to converge $k(T)$ with comparable accuracy. While the number of asymptotic initial channels below 1.6 eV is approximately 4000, it is likely that significantly fewer initial states would need to be propagated in order to obtain reasonable accuracy. (Recall from our discussion of Fig. 1 that we obtained very good $J=0$ ISSWP results using seven of the ten open channels for $E\leqslant 1.1$ eV, which is comparable to the number of TSWPs used.) However, we can be more confident that the TS-RWP approach leads to significant computational savings per propagation owing to the smaller grids and the use of just the real part of the wave packet. Furthermore, the present example, a rigorous, three-dimensional calculation including all relevant J and Coriolis coupling, naturally leads to the consideration of large numbers of TSWPs. Often, reasonably accurate cumulative reaction probabilities and rate constants can be obtained based on a $J=0$ or possibly some particular full or helicity decoupled $J>0$ result, coupled with J shifting ideas.[14,37,42] In such cases, far fewer TSWPs are required.

IV. CONCLUSIONS

We presented a ''transition state-real wave packet'' (TS-RWP) approach for obtaining the cumulative reaction probability $N(E)$ which combines Zhang and Light's transition state wave packet method[7] and the real wave packet formalism of Gray and Balint-Kurti.[24] Both these approaches can offer significant computational reductions in the estimation of cumulative reaction probabilities and the combined approach is expected to be particularly efficient. The implementation of the random superposition idea of Matzkies and Manthe[13] provides additional savings compared to summing over individually propagated wave packets. We illustrated the approach by estimating the cumulative reaction probability and thermal rate constants for the $D+H_2$ based on full dimensional calculations including all relevant angular momenta. It is also important to emphasize that the efficiencies afforded by both the transition state wave packet idea[7] and the random superposition idea[13] may be considerably im-

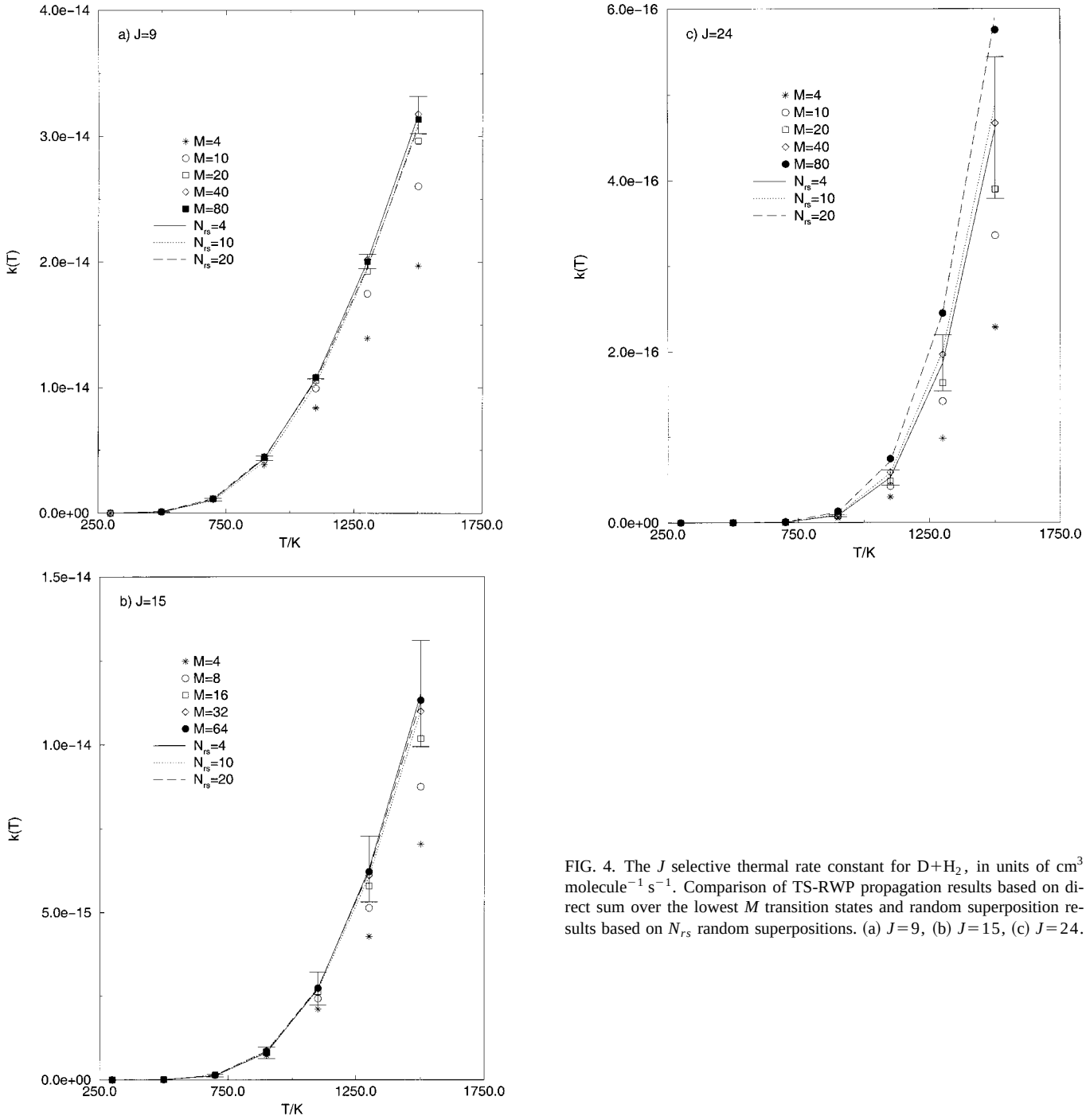

FIG. 4. The J selective thermal rate constant for $D+H_2$, in units of cm^3 $molecule^{-1}$ s^{-1}. Comparison of TS-RWP propagation results based on direct sum over the lowest M transition states and random superposition results based on N_{rs} random superpositions. (a) $J=9$, (b) $J=15$, (c) $J=24$.

proved by using a more appropriate coordinate system than the one we used in our illustration, e.g., one that mimics, in the vicinity of the transition state, the transition state normal coordinates.

Of course, as indicated in Sec. I, there are a variety of other approaches for obtaining $N(E)$, as well as also approaches for obtaining the rate constant without direct reference to $N(E)$. Depending on the information desired, these approaches might be less or more efficient than the approach outlined here. It is important to realize that all approaches (including our own) tend to be somewhat involved when problem sizes become so large that iterative linear algebra methods are required, and it is therefore difficult to make quantitative comparisons. While still involving complex vectors, for example, it might be that Manthe and Miller's reaction probability matrix approach[5] might be superior to the present approach if only a few energies E are of interest. (This approach, for each energy E, leads to a matrix eigenvalue problem that must be solved, perhaps by iterative matrix eigenvalue methods, for a certain number of eigenvalues.) If only a few temperatures, T, are of interest, it might be that a flux correlation approach would be most efficient.[31] (This approach involves propagation in complex time corresponding to a specific temperature.) We anticipate that the present approach might be most appropriate when a wide range of energies and temperatures is of interest, and possi-

TABLE II. Convergence of the TS-RWP rate constant for $J=9$, in units of cm^3 $molecule^{-1}$ s^{-1}. Numbers in brackets indicate powers of ten. N_{rs} refers to the number of random superpositions used in the calculations. $M=80$ (40 per parity) refers to the direct sum of the first 40 TS-RWPs. The corresponding accurate, GNVP results of Mielke *et al.* (Ref. 37) are also listed.

N_{rs}	300 K	500 K	700 K
4	2.78(−19)	8.88(−17)	1.08(−15)
10	1.48(−18)	8.78(−17)	1.00(−15)
20	2.04(−18)	1.18(−16)	1.17(−15)
40	1.78(−18)	1.16(−16)	1.17(−15)
$M=80$	5.49(−19)	1.07(−16)	1.15(−15)
GNVP	5.23(−19)	1.06(−16)	1.15(−15)

bly when the problem size becomes so large that the use of just real vectors makes the problem more tractable.

There are also correlation function based approaches to the cumulative reaction probability.[15,16,32] The approach of Ref. 32, for example, is similar in spirit to the Zhang and Light[7] (and thus our own) flux-based approach. It is interesting to note that one could combine this correlation function approach[32] with a simple identity or ''trick'' for obtaining correlation functions at time t given certain information at time $t/2$, as used in Refs. 49 and 50, to obtain an approach that involves similar computational effort to the present TS-RWP approach (i.e., instead of halving the wave packet size by utilizing just the real part as we have done, this would involve keeping complex wave packets but halving the propagation times.) Of course, the present TS-RWP approach still has more favorable computer memory requirements, and, in our view, is a little simpler to implement. However, it would be very interesting if the real wave packet ideas could be implemented within such correlation approaches, since then even greater computational savings *might* be achieved. It is not too difficult to cast the equations of Ref. 32 in real wave packet terms by invoking Eq. (14) and using relations such as Eq. (6) or the related identity Eq. (A11) of the Appendix. In fact, an approach similar to that of our Appendix, coupled with certain Chebyshev polynomial identities such as $T_{2k}=-T_0+2T_kT_k$, might yield both savings in terms of wave packet size and propagation time. We are currently investigating such possibilities.

While we demonstrated the feasibility of TS-RWP method with a nontrivial example, we intend to apply the scheme to more complicated problems in the future for which the advantages of the TS-RWP should be more pronounced relative to ISSWP formulations.

TABLE III. Comparison of TS-RWP, GNVP (Ref. 37) and experimental (Ref. 48) rate constants in units of cm^3 $molecule^{-1}$ s^{-1}. Numbers in brackets indicate powers of ten.

T(K)	TS-RWP	GNVP	Experiment
300	2.62(−16)±.01	2.76(−16)	2.96(−16)
500	3.13(−14)±.04	3.17(−14)	3.17(−14)
700	2.90(−13)±.07	2.92(−13)	3.07(−13)
900	1.09(−12)±.04	1.10(−12)	1.26(−12)
1100	2.63(−12)±.12	2.72(−12)	3.39(−12)
1300	4.99(−12)±.25	5.32(−12)	7.17(−12)

ACKNOWLEDGMENTS

This work was supported by the Office of Basic Energy Sciences, Division of Chemical Sciences, U.S. Department of Energy, under Contract No. W-31-109-ENG-38. Our thanks to Dr. D. G. Truhlar and Dr. S. L. Mielke for providing us with supplementary materials from their earlier work. We benefited from helpful conversations with Dr. E. M. Goldfield and Dr. A. J. H. M. Meijer.

APPENDIX

An alternative, more explicitly time-independent derivation of an equation very similar to Eq. (18), is presented here. This derivation is more in the spirit of time-independent wave packet ideas,[28,29] although we outline at the end how the result can be viewed as a special case of a more explicitly time-dependent argument similar to that of the main text.

With $f(E)=E_s=a_sE+b_s$, Eqs. (11) and (15) imply

$$N_i(E)=(2\pi\hbar)^2a_s^2\lambda\langle\phi_i(0)|\delta(E_s-H_s)\times F_{s_0}\delta(E_s-H_s)|\phi_i(0)\rangle. \tag{A1}$$

Expand the two delta function operators in Chebyshev polynomials $T_k(H_s)$,

$$\delta(E_s-H_s)=\sum_{k=0}^{\infty}c_k(E_s)T_k(H_s), \tag{A2}$$

with

$$c_k(E_s)=\frac{2}{\pi}\left[1-\frac{\delta_{k0}}{2}\right]\int_{-1}^{+1}\frac{dx}{\sqrt{1-x^2}}\delta(E_s-x)T_k(x)$$

$$=\frac{2}{\pi}\left[1-\frac{\delta_{k0}}{2}\right]\frac{T_k(E_s)}{\sqrt{1-E_s^2}}. \tag{A3}$$

Equation (A1) then becomes

$$N_i(E)=(2\pi\hbar)^2a_s^2\lambda\langle D_i|F_{s_0}|D_i\rangle, \tag{A4}$$

where

$$D_i=\sum_{k=0}^{\infty}c_k(E_s)(Q_i^{(k)}+iP_i^{(k)}). \tag{A5}$$

The $Q_i^{(k)}$ and $P_i^{(k)}$ satisfy Chebyshev separate recursions with $Q_i^{(0)}=\mathrm{Re}\,\phi_i(0)$, $Q_i^{(1)}=H_sQ_i^{(0)}$ generating $Q_i^{(k)}$, and $P_i^{(0)}=\mathrm{Im}\,\phi_i(0)$, $P_i^{(1)}=H_sP_i^{(0)}$ generating $P_i^{(k)}$. Including damping A of grid points in the reactant and product regions, these recursions are just like Eq. (8),

$$Q_i^{(k+1)}=A[-AQ_i^{(k-1)}+2H_sQ_i^{(k)}],$$
$$P_i^{(k+1)}=A[-AP_i^{(k-1)}+2H_sP_i^{(k)}], \tag{A6}$$

i.e., damped forward Chebyshev recursions as in the work of Mandelshtam and Taylor.[28]

Since F_{s_0} given by Eq. (12) is imaginary in the position representation, and $N(E)$ is real, Eq. (A4) may be written

$$N_i(E)=(2\pi\hbar)^2 a_s^2 \lambda i[\langle \mathrm{Re}\, D_i|F_{s_0}|\mathrm{Im}\, D_i\rangle - \langle \mathrm{Im}\, D_i|F_{s_0}|\mathrm{Re}\, D_i\rangle]. \quad \text{(A7)}$$

Because $\mathrm{Re}\, D_i$ and $\mathrm{Im}\, D_i$ are real basis functions, the imaginary antisymmetric property[43] of the flux operator implies $\langle \mathrm{Im}\, D_i|F_{s_0}|\mathrm{Re}\ D_i\rangle = -\langle \mathrm{Re}\, D_i|F_{s_0}|\mathrm{Im}\, D_i\rangle$, so that Eq. (A7) becomes

$$N_i(E)=(2\pi\hbar)^2 a_s^2 \lambda 2i\langle \mathrm{Re}\, D_i|F_{s_0}|\mathrm{Im}\, D_i\rangle. \quad \text{(A8)}$$

Finally, utilizing the explicit form of the flux operator, Eq. (12), one may show that

$$N_i(E)=\frac{(2\pi\hbar)^2}{\mu_s} a_s^2 \lambda \hbar \left[\left\langle \mathrm{Re}\, D_i \left| \frac{\partial}{\partial s} \mathrm{Im}\, D_i \right\rangle_{s=s_0} - \left\langle \frac{\partial}{\partial s} \mathrm{Re}\, D_i \right| \mathrm{Im}\, D_i \right\rangle_{s=s_0} \right], \quad \text{(A9)}$$

where, as with Eq. (18), the inner products are over all variables except the transition state coordinate which is held fixed at $s=s_0$. More explicitly, in terms of the Chebyshev iterates, Eq. (A9) is

$$N_i(E)=\frac{(2\pi\hbar)^2}{\mu_s} a_s^2 \lambda \hbar \left[\left\langle \sum_{k=0}^{\infty} c_k Q_i^{(k)} \left| \sum_{k'=0}^{\infty} c_{k'} \frac{\partial}{\partial s} P_i^{(k')} \right\rangle_{s=s_0} - \left\langle \sum_{k=0}^{\infty} c_k \frac{\partial}{\partial s} Q_i^{(k)} \left| \sum_{k'=0}^{\infty} c_{k'} P_i^{(k')} \right\rangle_{s=s_0} \right], \quad \text{(A10)}$$

which is very similar to Eq. (18) of the text. If one uses the explicit forms for the Chebyshev coefficients, c_k, given by Eq. (A3), for example, it is not too difficult to retrieve a prefactor proportionate to the one in Eq. (18).

There are differences between Eqs. (18) and Eq. (A10), but they are subtle. Equation (18) is based on the real part ($q_i^{(k)}$) of the forward and backward propagation of a complex initial condition $\phi_i(0)$, and this propagation is governed by the modified Schrödinger equation, Eq. (4) with $f(H)$ given by Eq. (7). In order for these propagations to be consistent with Eqs. (4) and (7), it is necessary to treat the first forward and first backward steps of the propagation in a special manner that involves evaluation of the action of a $\sqrt{1-H_s^2}$ operator, as outlined in the two paragraphs below Eq. (8). Equation (A10), on the other hand, involves the separate forward Chebyshev iterations of $\mathrm{Re}\ \phi_i(0)$ and $\mathrm{Im}\ \phi_i(0)$, given by $Q_i^{(k)}$ and $P_i^{(k)}$. While one can assert that $Q_i^{(k)}+iP_i^{(k)}$ is also a solution of the forward Chebyshev recursion, it is in fact not a solution of the modified Schrödinger equation owing to how $Q_i^{(1)}$ and $P_i^{(1)}$ are determined. While the connection with Schrödinger equation dynamics is thus less clear, the procedure for generating $Q_i^{(k)}$ and $P_i^{(k)}$ is a little simpler than that for generating the $q_i^{(k)}$, since one need not worry about evaluating the action of square root operators in evaluating the first forward and backward steps. We have also verified that Eq. (A10) gives results of comparable accuracy to Eq. (18).

The approach outlined in the main text is slightly more general, however, since Eq. (18) is a particular case of Eq. (17) which could be applied with, for example, $f(H)=H$, or possibly some other functional mapping of H. It is also possible to arrive at Eq. (A10) as a special case of a more general expression derived from the time-dependent arguments of the text. One simply repeats all the analysis of Sec. II B but instead of using the key relation Eq. (6), which allows complex wave packets $\phi(t)$ to be replaced by their real parts in Fourier integrals, one uses

$$I(f_E)=\int_{-\infty}^{+\infty} dt e^{-if_E t/\hbar}\phi(t) = 4\int_0^{+\infty} dt \cos(f_E t/\hbar)[Q(t)+iP(t)]. \quad \text{(A11)}$$

$Q(t)$ and $P(t)$ are the real parts of the forward time evolution, according to the modified Schrödinger equation, Eq. (4), of wave packets with initial conditions $Q(0)=\mathrm{Re}\,\phi(0)$ and $P(0)=\mathrm{Im}\,\phi(0)$. Notice that in both cases the initial condition is real. As with Eq. (6), it must be that $I(f_E)$ is one-sided. If the quantum dynamics is generated by Eq. (7), it is then not too difficult to recover an expression equivalent to Eq. (A10).

[1] W. H. Miller, J. Chem. Phys. **62**, 1899 (1975).
[2] W. H. Miller, S. D. Schwartz, and J. W. Tromp, J. Chem. Phys. **79**, 4889 (1983).
[3] T. Seideman and W. H. Miller, J. Chem. Phys. **96**, 4412 (1992).
[4] T. Seideman and W. H. Miller, J. Chem. Phys. **97**, 2499 (1992).
[5] U. Manthe and W. H. Miller, J. Chem. Phys. **99**, 3411 (1993).
[6] W. H. Miller, J. Phys. Chem. A **102**, 793 (1998).
[7] D. H. Zhang and J. C. Light, J. Chem. Phys. **104**, 6184 (1996).
[8] D. H. Zhang and J. C. Light, J. Chem. Phys. **106**, 551 (1997).
[9] D. H. Zhang, J. C. Light, and S.-Y. Lee, J. Chem. Phys. **109**, 79 (1998).
[10] D. H. Zhang and J. C. Light, Faraday Discuss. **110**, 105 (1998).
[11] X. T. Wu and E. F. Hayes, J. Comput. Phys. **130**, 136 (1997).
[12] O. I. Tolstikhin, V. N. Ostrovsky, and H. Nakamura, Phys. Rev. Lett. **80**, 41 (1998).
[13] F. Matzkies and U. Manthe, J. Chem. Phys. **110**, 88 (1988).
[14] J. M. Bowman, J. Phys. Chem. **95**, 4961 (1991).
[15] S. Garashchuk and D. J. Tannor, J. Chem. Phys. **109**, 3028 (1998).
[16] S. Garashchuk and D. J. Tannor, J. Chem. Phys. **110**, 2761 (1999).
[17] S. Garashchuk and D. J. Tannor, Phys. Chem. Chem. Phys. **1**, 1081 (1999).
[18] J. V. Lill, G. A. Parker, and J. C. Light, Chem. Phys. Lett. **89**, 483 (1982).
[19] J. T. Muckerman, Chem. Phys. Lett. **173**, 200 (1990).
[20] D. T. Colbert and W. H. Miller, J. Chem. Phys. **96**, 1982 (1992).
[21] V. Szalay, J. Chem. Phys. **105**, 6940 (1996).
[22] R. Kosloff and D. Kosloff, J. Comput. Phys. **63**, 363 (1986).
[23] D. Neuhauser and M. Baer, J. Chem. Phys. **91**, 4651 (1989).
[24] S. K. Gray and G. G. Balint-Kurti, J. Chem. Phys. **108**, 950 (1998).
[25] J. H. M. Meijer, E. M. Goldfield, S. K. Gray, and G. G. Balint-Kurti, Chem. Phys. Lett. **293**, 271 (1998).
[26] H. Tal-Ezer and R. Kosloff, J. Chem. Phys. **81**, 3967 (1984).
[27] S. K. Gray, J. Chem. Phys. **96**, 6543 (1992).
[28] V. A. Mandelshtam and H. S. Taylor, J. Chem. Phys. **103**, 2903 (1995).
[29] Y. Huang, S. S. Iyengar, D. J. Kouri, and D. K. Hoffman, J. Chem. Phys. **105**, 927 (1996).
[30] G. G. Balint-Kurti, A. I. Gonzalez, E. M. Goldfield, and S. K. Gray, Faraday Discuss. **110**, 169 (1998).
[31] W. H. Thompson and W. H. Miller, J. Chem. Phys. **102**, 7409 (1995).
[32] S. M. Miller and T. Carrington, Jr., Chem. Phys. Lett. **267**, 417 (1997).
[33] S. J. Jeffrey and S. C. Smith, Chem. Phys. Lett. **278**, 345 (1997).
[34] P. Siegbahn and B. Liu, J. Chem. Phys. **68**, 2457 (1978).
[35] D. G. Truhlar and C. J. Horowitz, J. Chem. Phys. **68**, 2466 (1978).
[36] D. G. Truhlar and C. J. Horowitz, J. Chem. Phys. **71**, 1514 (1979).

[37] S. L. Mielke, G. C. Lynch, D. G. Truhlar, and D. W. Schwenke, J. Phys. Chem. **98**, 8000 (1994).
[38] R. T Pack, J. Chem. Phys. **60**, 633 (1974).
[39] E. M. Goldfield and S. K. Gray, Comput. Phys. Commun. **98**, 1 (1996).
[40] A. J. H. M. Meijer and E. M. Goldfield, J. Chem. Phys. **108**, 5404 (1998).
[41] C. Leforestier, J. Chem. Phys. **94**, 6388 (1991).
[42] S. K. Gray, E. M. Goldfield, G. C. Schatz, and G. G. Balint-Kurti, Phys. Chem. Chem. Phys. **1**, 1141 (1999).
[43] T. J. Park and J. C. Light, J. Chem. Phys. **88**, 4897 (1988).
[44] T. Seideman and W. H. Miller, J. Chem. Phys. **95**, 1768 (1991).
[45] W. H. Press, B. P. Flannery, S. A. Teukolsky, and W. T. Vetterling, *Numerical Recipes: Art of Scientific Computing* (Cambridge University Press, Cambridge, 1986), p. 342.
[46] D. C. Sorensen, SIAM J. Matrix Anal. Appl. **13**, 357 (1992).
[47] See the ARPACK homepage, http://www.caam.rice.edu/software/ARPACK/
[48] J. V. Michael and J. R. Fisher, J. Phys. Chem. **94**, 3318 (1990).
[49] F. Matzkies and U. Manthe, J. Chem. Phys. **108**, 4828 (1998).
[50] U. Manthe and F. Matzkies, Chem. Phys. Lett. **282**, 442 (1998).